Available online at www.sciencedirect.com
SCIENCE DIRECT®
Journal of Catalysis 227 (2004) 148–163
JOURNAL OF CATALYSIS
www.elsevier.com/locate/jcat

Synthesis and characterization of carbometallated palladacycles over 3-hydroxypropyltriethoxysilyl-functionalized MCM-41

C. Venkatesan, A.P. Singh *

Catalysis Division, National Chemical Laboratory, Pune 411 008, India

Received 7 April 2004; revised 26 June 2004; accepted 30 June 2004

Available online 5 August 2004

Abstract

Heterogeneous carbometallated palladacycle catalysts have been synthesized by treatment of palladation reagents with 3-hydroxypropyltriethoxysilane-incorporated MCM-41 (OH-M) under mild reaction conditions. Palladation over organo-functionalized MCM-41 and organo-functionalized silica has been performed and it was found that the spatial confinement induced by the pore walls of organo-functionalized MCM-41 forces the propyl group to cyclize in the presence of an electrophilic metal center which is found to be much lower in organo-functionalized silica. Optimization studies, including change in Pd concentration in solution, different palladation reagents in palladation reactions such as Li_2PdCl_4, $Pd(OAc)_2$, effect of base, palladation temperature, and different solvents (methanol, chloroform, and acetone used as reaction medium), have been performed over organo-functionalized MCM-41 for obtaining better results of palladation. A number of characterization techniques have been exploited to support the formation of a palladacycle complex inside the pores of mesoporous materials. The Heck alkenylation reaction, which is universally accepted as a sharpening stone of palladium catalysts, was set as a model reaction to evaluate the catalytic activity of all the catalysts investigated in this study. The heterogeneity of the catalyst has also been studied.

Keywords: Carbometallation; Palladacycles; MCM-41; Heck reaction; Bromobenzene

1. Introduction

The carbon–carbon bond-forming reaction is a potential application of palladium catalysts [1]. Among a pool of palladium catalysts, carbometallated Pd(II) compounds, especially palladacycles, have emerged as very promising catalysts for C–C bond-forming reactions [2–5]. Cyclopalladated phosphines, phosphinite, chelating diphosphines, carbene ligands, and dimethylglycine have also been reported [6–9]; however, for commercial use it has drawbacks as the catalysts require either hazardous phosphate ligands for the stabilization of Pd in its zero valence state or tedious synthesis and activation procedures. A recent trend in catalysis because of environmental and economic concerns is the transformation of a homogeneous catalytic system into a heterogeneous system in which the active centers are supported on a solid, making the catalyst easily recoverable from the reaction mixture with the possibility of reuse and waste minimization [10–12]. For this reason, the activities of Pd and its metallic complexes supported over variety of solid supports, particularly active charcoal, silica, and inorganic oxides, have been studied for C–C coupling reactions [13–18]. Pd-modified zeolites have been studied in the Heck reaction [19,20], but the smaller pore dimension limits their application for larger molecules. Moreover, Pd-zeolite catalysts need to be activated to get the active metallic Pd in zero state.

The discovery of mesoporous molecular sieves has simulated a renewed interest in developing adsorbents and sensors and designing catalysts due to their high surface areas with narrow pore-size distributions (2–20 nm) [21,22]. Kosslick et al. have studied the anchoring of alkylsilylsulfonic acid into the walls of Al-MCM-41 to stabilize the catalytically active palladium complex that was formed dur-

* Corresponding author. Fax: +91-20-25893761.
E-mail address: apsingh@cata.ncl.res.in (A.P. Singh).

0021-9517/$ – see front matter
doi:10.1016/j.jcat.2004.06.026

ing the course of reaction [23]. Silica-supported palladacycle catalysts have been studied for C–C coupling reactions [24,25]. Corma and co-workers have reported an oxime–carbapalladacycle complex covalently anchored to silica as an active and reusable heterogeneous catalyst for Suzuki cross-coupling in water [26]. Various attempts toward the immobilization of organometallic complexes have been made previously, such as attachment to the support materials by chemisorption, immobilization by steric hindrance in zeolite micropores (ship-in-a-bottle concept), or supported liquid-phase catalysts [27].

ortho-Palladation with the weakest palladation agent (Li_2PdCl_4) under very mild conditions, due to steric promotion of an aromatic C–H bond activation, was studied by Dunia et al. [28]. In this study, carbometallation was used to immobilize the palladium catalysts on MCM-41 support. Carbometallation of anchored ligands with palladium metal centers enhanced by steric constraint of the mesopores has been exploited to obtain heterogeneous palladium catalysts. Recently, we have reported for the first time that aliphatic C-metallated palladacycle was synthesized in the pores of 3-hydroxypropyltriethoxysilane-functionalized MCM-41 and found as an active and stable catalyst for Heck alkenylation of bromobenzene [29]. Here we report the synthesis and characterization of palladacycle-MCM-41 materials along with the catalysts textural properties, and the influence of synthesis conditions on the catalytic performance of the catalysts in the Heck alkenylation of bromobenzene. The heterogeneity of the catalyst has also been examined.

2. Experimental

2.1. Materials

Tetraethylorthosilicate (TEOS, Aldrich, USA), 3-chloropropyltriethoxysilane (3-ClPTS, Aldrich), 3-aminopropyltriethoxysilane (APTES, Lancaster, UK), cetyltrimethylammonium bromide (C_{16}TAB, Loba Chemie, India), tetramethylammonium hydroxide (TMAOH, 25% solution in water, Aldrich), palladium acetate (Aldrich), palladium chloride, lithium chloride, sodium chloride, methanol, ethanol, ammonia, chloroform, acetone, and sodium acetate (Loba Chemie) were used as the reagents for the synthesis of catalysts. Styrene (Aldrich), bromobenzene (BB), potassium carbonate, and 2-methyl-*N*-pyrrolidone (s–d fine chemicals, India) were used as such without further purification.

2.2. Synthesis of Cl-MCM-41 (Cl-M)/OH-MCM-41 (OH-M)

3-ClPTS-functionalized MCM-41 has been prepared by cocondensation of TEOS with 3-ClPTS. Prior to this work, in the synthesis of 3-aminopropyltriethoxysilane-functionalized MCM-41, we have observed that the use of a surfactant (C_{16}TAB) with TMAOH and evaporation of the alcohol prior to gel refluxing strongly improve the ordering of the functionalized MCM-41 materials [30]. Therefore, we have applied the same synthesis approach in this work. Synthesis gels of the general molar composition $(1 - x)$ TEOS:x 3-ClPTS:0.25 C_{16}TAB:0.3 TMAOH:10 MeOH:90 H_2O were prepared. The details of chemical compositions for the synthesis gels are given in Table 1. In a typical synthesis procedure, TEOS (25.0 g) and 3-ClPTS (0.84 g) in methanol were added dropwise with stirring to an aqueous solution of TMAOH (13.5 g) and C_{16}TAB (11.24 g). The mixture was stirred at room temperature for 5 h and then transferred into a glass reactor and refluxed at 373 K for 48 h. The product was filtered, washed with excess deionized water, and dried at 373 K for 10 h. The organic surfactant molecules were removed by refluxing with acid solvent mixture (100 ml methanol + 5 ml HCl/g of solid material) at 343 K for 24 h.

Chlorine groups in the Cl-M sample were hydrolyzed into hydroxyl groups by treating 1 g of the extracted sample with 10 ml of H_2O and 10 ml of MeOH at 338 K for 2 h. The hydrolyzed material (OH-M) was filtered and dried at 373 K for 10 h.

2.3. Preparation of Cl/OH–SiO_2

3-ClPTS-functionalized silica was obtained by a one-step, base-catalyzed procedure to obtain 20 wt% of 3-ClPTS in a dry sample. The molar ratio of the compound was: 0.9 SiO_2:0.1 ClPTS:8 EtOH:3 H_2O:0.008 NH_3. Wet gel was

Table 1
Molar composition of silylating agent and coupling agents in the synthesis of mesoporous materials with the molar composition: $(1 - x)$ TEOS:x 3-ClPTS: 0.25 C_{16}TAB:0.3 TMAOH:90 H_2O:10 MeOH

Catalysts	TEOS (mol)	3-ClPTS (mol)	x		3-ClPTS (mmol/g)		% of loading of 3-ClPTS	Surface area (m^2/g)
			Input	Output[a]	Input	Output[a]		
Cl-M0	0.1	0	0	0	–	–	–	1050
Cl-M1	0.12	0.003	0.024	0.016	0.42	0.27	64	760
Cl-M2	0.107	0.007	0.061	0.036	1.08	0.6	56	735
Cl-M3	0.093	0.01	0.097	0.059	1.78	0.99	56	855
Cl-M4	0.08	0.013	0.14	0.1	2.7	1.67	62	614
Cl-M5	0.067	0.017	0.202	0.159	4.21	2.65	63	726
Cl-M6	0.05	0.02	0.286	0.196	6.66	3.26	49	715

[a] Calculated from the data obtained from C and H analysis.

prepared as follows. First two solutions were prepared at room temperature: solution A contained TEOS, 3-ClPTS, and half of the total ethanol content whereas solution B consisted of the remaining ethanol, water, and ammonium hydroxide. Solution A was added to B under stirring and the resulting sol was heated to 50 °C. The gelation took place in 1 h. The resulting alcogel was dried slowly under cover at room temperature to obtain 3-ClPTS-functionalized silica materials (Cl–SiO_2). The Cl–SiO_2 was treated with aqueous methanol for 2 h to convert all the Cl groups into OH groups (OH–SiO_2).

2.4. Preparation of palladacycle MCM-41 (Pd-OMS)/ palladacycle–SiO_2 (Pd–SiO_2)

Palladation was carried out over the samples OH-M/OH–SiO_2 with the palladation reagent, Li_2PdCl_4, NaOAc in methanol/acetone, or Pd $(OAc)_2$ in $CHCl_3$ either at reflux temperature or at room temperature for 24 h. After palladation, the gray color material was washed thoroughly with aqueous methanol to remove all unreacted palladium salt and the inorganic base. Different concentrations of Li_2PdCl_4 have been used for the palladation of OH-M to get different concentrations of Pd-loaded catalysts.

2.5. Preparation of Am-MCM-41 and Am-PdMS

The molar composition of the synthesis mixture was as follows: 0.8 TEOS:0.2 APTES:0.125 $(CTMA)_2O$:0.15 $(TMA)_2O$:90 H_2O:10 MeOH. TEOS (16.6 g) and APTES (4.4 g) in methanol (32.0 g) were added drop wise for 20 min with stirring to an aqueous solution of TMAOH (10.9 g) and CTMABr (9.1 g). The mixture was stirred at room temperature for 4 h and then transferred into a glass reactor and refluxed at 373 K for 48 h. The product was filtered, washed with excess deionized water, and dried at 373 K for 10 h. The organic surfactant molecules were removed by refluxing with acid solvent mixture (100 ml methanol + 5 ml HCl/g of solid material) at 343 K for 24 h.

Am-PdMS (1.0 g, 1 mmol N/g) was prepared by treating Am-MCM-41 with $Pd(OAc)_2$ (1 mmol) in chloroform at 335 K for 24 h. The orange-colored material was obtained by centrifuging the solution.

3. Characterization of catalysts

Synthesized catalysts were characterized by X-ray diffraction using a Rigaku Miniflex powder diffractometer on finely powdered samples using Cu-K_α radiation and 45 kV and 40 mA. The scans were done at 2° per minute. The XRD patterns were recorded for 2θ's between 1.5° and 50°.

Palladium content in the catalysts was determined using inductively coupled plasma-optical emission spectra (ICP-OES) on a Perkin–Elmer P1000 instrument. An average of two analyses was done to calculate the Pd content present in the samples. Samples for ICP-OES analyses were prepared by dissolving 0.05 g of sample in approximately 5 ml of HF and subsequently with 5 ml of aqua regia and then diluted to 50 ml with deionized water. Analyses of the organic content present in the catalysts were carried out using a Carlo-Erba C, H, and N analyzer.

Adsorption of nitrogen was carried out at 77 K using a NOVA 1200 (Quantachrome) apparatus for analyzing surface areas and pore-size distributions of the synthesized catalysts. Specific surface areas were calculated following the BET procedure. Pore-size distribution was obtained by using BJH pore analysis applied to the desorption branch of the nitrogen adsorption/desorption isotherms.

The FTIR spectra were recorded on a Perkin–Elmer Spectrum One FT-IR spectrometer using a diffuse reflectance scanning disk technique. The spectra of solid samples diluted with anhydrous KBr were recorded at room temperature in the transmission mode, in the range 4000 to 450 cm^{-1} at 4 cm^{-1} resolutions.

Thermogravimetric analyses (TGA and DTA) were performed using a Mettler Toledo 851^e instrument, from 303 to 1173 K at a heating rate of 20 K/min under air flow.

The scanning electron microscope (SEM) photographs of the samples were obtained using a Leica Stereoscan 440 instrument.

Solid-state ^{13}C spectra of OH-M5 and Pd-OMS5 and ^{29}Si CP MAS NMR spectra of OH-M5 and Pd-OMS5 were recorded on a Bruker DRX-500 NMR spectrometer spun at 8 kHz. Liquid-state ^{13}C NMR spectra were recorded on a Bruker DRX-300 NMR spectrometer.

X-ray photoelectron spectra (XPS) were obtained using a VG Microtech Multilab-ESCA-3000 spectrometer equipped with a twin anode of Al and Mg. All the measurements are made on as-received powder samples using Mg-K_α X-ray at room temperature. Base pressure in the analysis chamber was 4×10^{-10} Torr. A multichannel detection system with nine channels is employed to collect the data. The overall energy resolution of the instrument is better than 0.7 eV, determined from the full width at half-maximum of the $4f_{7/2}$ core level of a gold surface. The errors in all BE (binding energy) values were with in ±0.1 eV.

The diffuse reflectance UV–vis spectra in the 200–800 nm ranges were recorded with a Shimadzu UV-2101 PC spectrometer equipped with a diffuse reflectance attachment using $BaSO_4$ as a reference.

Heck alkenylation reactions (Scheme 2) were carried out in a 25-ml glass reactor. In a typical experiment 0.03 g catalyst and 2.4×10^{-3} mol potassium carbonate were added into a solution of 2×10^{-3} mol bromobenzene and 3×10^{-3} mol of styrene in 5.0 ml *N*-methyl-2-pyrrolidone solvent. The reaction mixture was heated under stirring for a specified time. At regular intervals samples were collected and analyzed by GC (HP 6890 N series) equipped with a FID detector and HP-5 capillary column. Peak positions of reaction products were compared and matched with the retention

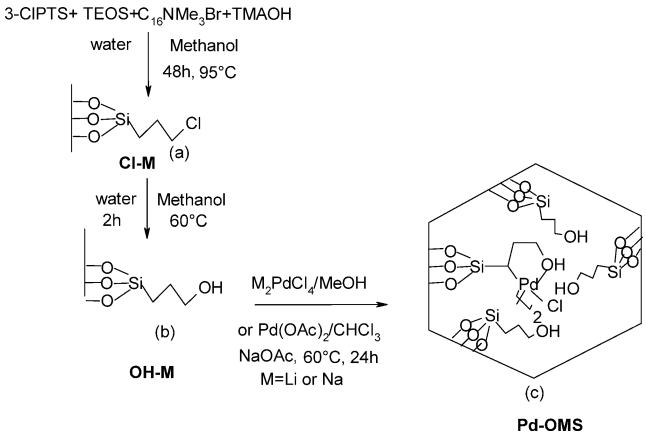

Scheme 1.

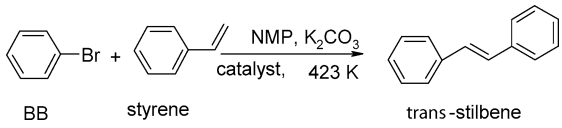

Scheme 2.

times of authentic samples. The identity of the products was also confirmed by GC-MS and ^{1}H NMR analysis.

4. Results and discussion

4.1. Synthesis

The generalized synthesis procedure of palladacycle over MCM-41 is outlined in Scheme 1. In order to immobilize the homogeneous catalyst on a heterogeneous solid surface, an organic linker group is needed. Organic functionalization of the internal surfaces of MCM-41 can be achieved, either by covalently grafting of various organic species onto the surface or by incorporating of functionalities directly during the preparation. The organosilane having ligands such as chlorine or amine is directly grafted to the silica surface by an in situ silylation procedure. The chlorine functional group is hydrolyzed into the hydroxyl group either under synthesis condition or at postsynthesis hydrolysis treatment. These types of ligands permit formation of complexes through coordination bonds with metal centers [31,32]. There are three types of ≡SiOH groups over a siliceous MCM-41 surface [33], e.g., isolated single, hydrogen bonded, and geminal ≡SiOH groups, only the single and geminal ≡SiOH groups of which are responsible for active silylation. The hydrolysis of the required composition of 3-ClPTS and TEOS (0.05–0.3 and 0.095–0.7, respectively) in the presence of TMAOH enriches the mother liquor with single and geminal ≡SiOH monomer silica species. Cocondensation of symmetrical $Si(OH)_4$ and unsymmetrical $RSi(OH)_3$ species results in the formation of uniformly distributed organofunctionalized silica.

Six different molar ratios of TEOS to 3-ClPTS in the synthesis mixture have been taken to obtain materials with a range of concentrations of 3-ClPTS functional groups over MCM-41. Six different samples are designated as Cl-M1, Cl-M2, Cl-M3, Cl-M4, Cl-M5, and Cl-M6 and the respective hydrolyzed samples are designated as OH-M1, OH-M2, OH-M3, OH-M4, OH-M5, and OH-M6. The fraction of functionalized silicon atoms in the synthesis gel (x) was set in the range of 0.025 to 0.3 as it was reported that material prepared with a fraction of silicon atoms in that range is more stable and hydrophobic in nature because of the hydrophobization of all the silanol groups. The higher fraction of functionalized silicon atoms obtained in the synthesized material was 0.2 (Table 1). From C and H elemental analysis it was observed that effective loading of 3-ClPTS groups into the coupling agent, TEOS, was about 60 wt% with respect to the amount of 3-ClPTS taken in the synthesis gel.

Palladation was carried out over OH-M1, OH-M2, OH-M3, OH-M4, OH-M5, and OH-M6 samples under similar reaction conditions to obtain Pd-OMS1, Pd-OMS2, Pd-OMS3, Pd-OMS4, Pd-OMS5, and Pd-OMS6, respectively. All the palladation reactions were carried out at 335 K in methanol and with sodium acetate (Table 3). Dunia et al. have achieved the best results when *ortho*-palladation of a sterically crowded primary benzylamine, α-phenylneopentylamine was performed with Li_2PdCl_4 and excess sodium acetate in methanol [28]. Polar solvents have some advantages over nonpolar solvents in the palladation reactions due to their strong solvating effect that assists in the generation of a three-coordinate intermediate of the $[L_2PdX_2(solv)]$ type required for subsequent C–H bond activation [34]. Here the same steric effect due to the organofunctionalized mesoporous structure has been utilized for the activation of aliphatic C–H activation. Formation of a quasi-immobilized palladium complex inside the mesopores when the anchored 3-hydroxypropyltriethoxy silane is treated with palladium source creates a steric constraint which might be expected to cause aliphatic C–H bond activation and hence carbometallation occurs with the weakest of palladation reagents and weak ligands under mild conditions. In the case of porous catalysts incorporating with organic functionalities, not only the constraint of the surface but also of the pore itself must be considered, potentially resulting in an even larger constraint [35]. The spatial confinement induced by the pore walls forces the propyl group to cyclize in the presence of an electrophilic metal centre. Two main possible factors determine the easier aliphatic carbometallation with weakest palladation reagents: (i) a large effective volume of the ligand (3-hydroxypropyltriethoxysilane) incorporated into MCM-41 pore walls must increase an internal energy of the intermediate binuclear coordination compounds due to a set of unfavorable nonbonding interactions [36], thus stimulating an intermediate dissociation to form a reactive three-coordinate species; (ii) the same steric effect must result in a weakening of Pd–O bond in the coordination intermediate, to make the palladium(II) center more electrophilic. Both

effects essentially facilitate the C–H bond activation [37]. The palladation results obtained with the weak palladation reagent, Li_2PdCl_4, in methanol in the presence of sodium acetate at room temperature may be considered as the most convincing evidence for the mesoporous structure-promoted aliphatic C–H bond activation.

Few samples were prepared with or without addition of base and at room temperature to study the effect of base and synthesis temperature. Chloroform or acetone has also been used instead of methanol but it was found that Li_2PdCl_4 was not dissolving in chloroform. Palladium acetate was taken as the palladium source in chloroform solvent. The textural properties along with the physicochemical activities of the synthesized catalysts are given in Tables 2 and 3. The different conditions in the preparation of different palladacycle catalysts are also given in Table 4. For comparison, 3-aminopropylated MCM-41 (Am-MCM-41) has been palladated with $Pd(OAc)_2$ under similar reaction conditions to get Am-PdMS catalysts and the characterization data are compared with Pd-OMS-54 catalysts. Palladation of 3-aminopropyltriethoxysilane with $Pd(OAc)_2$ in $CDCl_3$ solvent has been performed and analyzed by liquid-phase

Table 2
Physical characteristics of the catalysts (OH-M)

Catalysts	2θ (°)	d_{100} (Å)	Unit-cell parameter, a_0 (Å)	BET surface area (m^2/g)
OH-M1	2.57	34.36	39.68	547
OH-M2	2.49	35.47	40.96	578
OH-M3	2.47	35.75	41.29	862
OH-M4	2.48	35.61	41.12	624
OH-M5	2.34	37.74	43.58	732
OH-M6	2.40	35.9	41.46	712

Table 3
Physicochemical characteristics of the catalysts (Pd-OMS)

Catalysts	2θ (°)	d_{100} (Å)	Unit-cell parameter, a_0 (Å)	BET surface area (m^2/g)	Pd content (wt%)	Conversion of BB (wt%)[g]	Selectivity *trans*-stilbene (%)	TON[h]
Pd-OMS1[a]	2.62	33.71	38.93	351	0.44	5.8	100	93
Pd-OMS2[a]	2.76	32.0	36.95	384	0.88	27.3	95	205
Pd-OMS3[a]	2.77	31.88	36.82	632	0.94	33.8	90	213
Pd-OMS4[a]	2.40	36.83	42.53	640	1.12	42.4	89	340
Pd-OMS5[a]	2.49	39.42	40.96	862	1.05	57.8	90	389
Pd-OMS6[a]	2.4	35.9	41.46	722	0.97	38.5	92	280
Pd-OMS51[b]	2.32	38.07	43.96	590	0.32	71.1	90.0	1570
Pd-OMS52[c]	2.36	37.42	43.21	605	0.35	86.6	90.0	1748
Pd-OMS53[d]	2.34	37.74	43.58	723	0.26	76.6	90.0	2082
Pd-OMS54[e]	2.38	37.1	42.85	894	0.38	53.6	90.0	997
Pd-OMS55[f]	2.44	36.2	41.8	802	0.71	74.0	91	736
Pd-Si-MCM-41 (CM0)	2.86	30.9	35.66	1020	0.14	No reaction	–	–
SiO_2–Pd[a]	–	–	–	255	0.26	5.6	100	152

[a] OH-M1, OH-M2, OH-M3, OH-M4, OH-M5, OH-M6, and OH–SiO_2, respectively, = 1 g; $Li_2PdCl_4 = 1.4 \times 10^{-4}$ mol (1.5 wt% Pd); NaOAc = 50 mg; methanol = 20 ml; reaction temperature = 335 K; reaction time = 24 h.
[b] OH-M5 = 1.0 g; $Li_2PdCl_4 = 1.4 \times 10^{-4}$ mol; NaOAc = 0.05 g; methanol = 20 cc; reaction temperature = 303 K; reaction time = 24 h.
[c] OH-M5 = 1.0 g; $Li_2PdCl_4 = 1.4 \times 10^{-4}$ mol; methanol = 20 cc; reaction temperature = 335 K; reaction time = 24 h.
[d] OH-M5 = 1.0 g; $Li_2PdCl_4 = 1.4 \times 10^{-4}$ mol; acetone = 20 cc; reaction temperature = 335 K; reaction time = 24 h.
[e] OH-M5 = 1.0 g; $Pd(OAc)_2 = 1.4 \times 10^{-4}$ mol; chloroform = 20 cc; reaction temperature = 335 K; reaction time = 24 h.
[f] OH-M5 = 1.0 g; $Pd(OAc)_2 = 1.4 \times 10^{-4}$ mol; NaOAc = 0.05 g; chloroform = 20 cc; reaction temperature = 335 K; reaction time = 24 h.
[g] BB = 2 mmol; styrene = 3 mmol; K_2CO_3 = 2.4 mmol; NMP = 5.0 ml; temperature = 423 K; catalyst = 30 mg; reaction time = 5 h.
[h] TON (turnover number) = moles of BB converted per mole of Pd.

Table 4
Effect of Pd loading (wt%)

Catalysts[a]	Surface area (m^2/g)	Pd content (wt%)[b]		Conversion of BB (wt%)[c]	Selectivity *trans*-stilbene (%)	TON[d]
		Input	Output			
Pd-OMS5 (0.33)	911	0.48	0.33	18.8	100	403
Pd-OMS5 (0.62)	863	0.9	0.62	37.8	91.0	431
Pd-OMS5 (1.05)	862	1.5	1.05	57.8	92.0	389
Pd-OMS5 (1.4)	763	3.0	1.40	90.1	91.0	455
Pd-OMS5 (1.68)	887	6.0	1.68	70.0	100	291

[a] Number in parentheses denotes the Pd content (wt%) present in the catalyst.
[b] Input is based on the amount of Pd in solution during palladation reaction; output is based on the ICP-OES analysis.
[c] BB = 2 mmol; styrene = 3 mmol; K_2CO_3 = 2.4 mmol; NMP = 5.0 ml; temperature = 423 K; catalyst = 30 mg; reaction time = 5 h.
[d] TON (turnover number) = moles of BB converted per mole of Pd.

^{13}C NMR spectra and diffuse reflectance UV–vis spectra. The results are compared with the solid sample prepared with Am-MCM-41.

4.2. X-ray diffraction (XRD)

The XRD patterns of the as-synthesized samples show an intense peak due to d_{100} reflection, at 2θ between 2.0 and 2.5° accompanied by weaker reflections at 2θ between 4.0°and 6.5°, corresponding to the d_{110}, d_{200}, and d_{210} spacing (hexagonal symmetry p6mm) which are characteristic peaks of MCM-41 [21]. The XRD peak intensity of template-extracted and hydrolyzed OH-M1 and OH-M2 decreased significantly as compared to the peak intensity of Cl-M1 and Cl-M2, respectively. Likewise the peak intensity of Pd-OMS1 and Pd-OMS2 catalysts decreased further when compared to the peak intensity of OH-M1 and OH-M2, respectively (Fig. 1). As can be seen from Table 1 the fraction of organo-functionalized atoms over Cl-M1 and Cl-M2 is lower and hence might have left more silanol groups free. While treating the catalysts with acidic solvents in the case of template extraction and basic solvents in the case of palladation reaction, the active Si–O bond in ≡SiOH hydrolyzed easily and hence the long-range order of the structure collapsed as reflected in the XRD pattern (Fig. 1). On the other hand, OH-M3, OH-M4, OH-M5, and respective palladated materials Pd-OMS3, Pd-OMS4, and Pd-OMS5 retain their long-range order after palladation as seen in X-ray diffraction (Fig 2). As the concentration of the organo-functional group increases the surface of the silica walls become more passive due to the silylation, which help in retaining the long-range order during reaction with acidic or basic solvents. The unit cell parameter ($a_0 = 2d_{100}/\sqrt{3}$) of the palladated materials is close to 40 Å (Table 3).

The XRD pattern of palladium metal has major diffraction peaks at $2\theta = 40.0°$ (111) and 46.5° (200), which are found for Pd-OMS catalysts prepared with Li_2PdCl_4 and NaOAc in methanol at 335 K, confirming the presence of bulk Pd on the surface apart from metallated palladium (Fig. 3). Fig. 4 shows the XRD pattern of OH-M-5, which is palladated with different amounts of Pd under similar reaction conditions (Pd-OMS5 series). It was observed that when the loading of Pd is lower, there was no diffraction pattern of metallic Pd observed. As the loading increases the diffraction pattern corresponding to the Pd rises. At higher loadings of Pd (Pd-OMS5 (1.4) and Pd-OMS5 (1.68)) the peak intensity corresponding to Pd is higher. This shows that as the concentration of Pd increases while loading the chance for depositing bulk Pd at the surface also increases.

Palladation of OH-M5 with Li_2PdCl_4 and sodium acetate in methanol either at room temperature or at 335 K produces bulk Pd^0 on the surface as evidenced by the XRD pattern. Base added during palladation catalyzes the formation of palladacycle and also the deposition of Pd as bulk on the surface of silica. Catalysts prepared with different solvents such as methanol (Pd-OMS52), acetone (Pd-OMS53), and chloroform (Pd-OMS54) with Li_2PdCl_4 at 335 K without addition of base showed no characteristic Pd peak (Fig. 5). Pd-OMS54 prepared with $Pd(OAc)_2$ in $CHCl_3$ at 335 K shows no Pd^0 peaks but the same when prepared with sodium acetate shows Pd^0 peaks. These results suggest that formation of palladacycle and deposition of bulk Pd on the surface mainly depend on the solvents and base used. It was found that the propyl alcohol acts as a ligand in which the loan pair of electrons on oxygen atoms coordinates with palladium which in turn coordinates with the carbon atom of the propyl chain by cyclization under very mild conditions without formation of any bulk Pd at the silica surfaces.

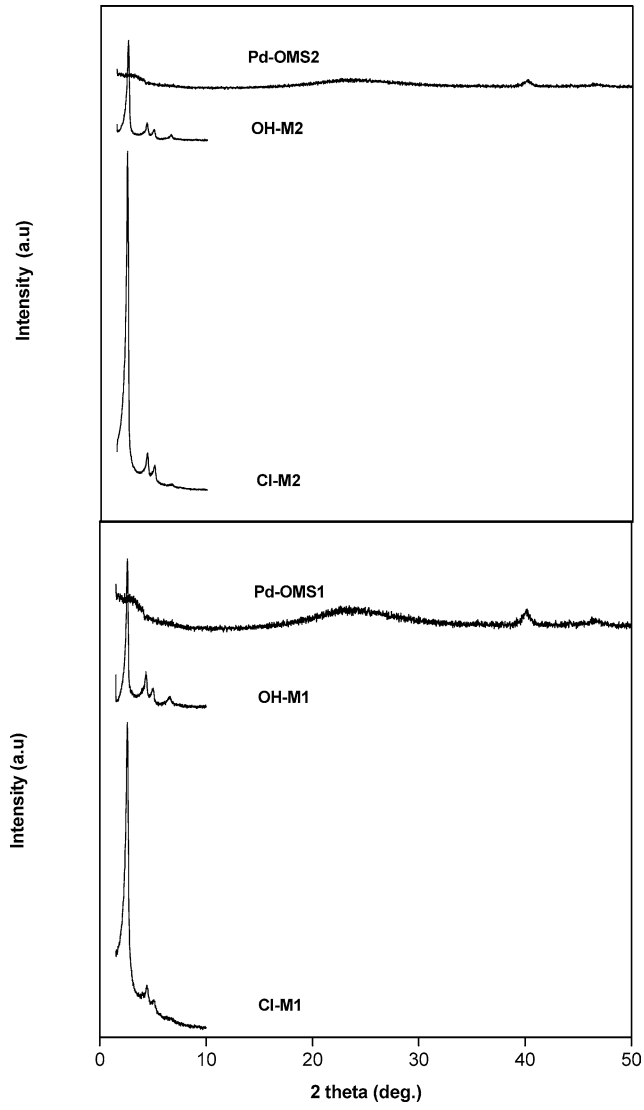

Fig. 1. X-ray diffraction patterns of Cl-M, OH-M, and Pd-OMS.

4.3. ICP-OES and CHN analyses

The palladium content in the materials was determined by ICP-OES analysis. When similar concentrations of Pd (1.5 wt% Pd) were treated with OH-M samples with different concentrations of 3-ClPTS, the uptake of Pd through

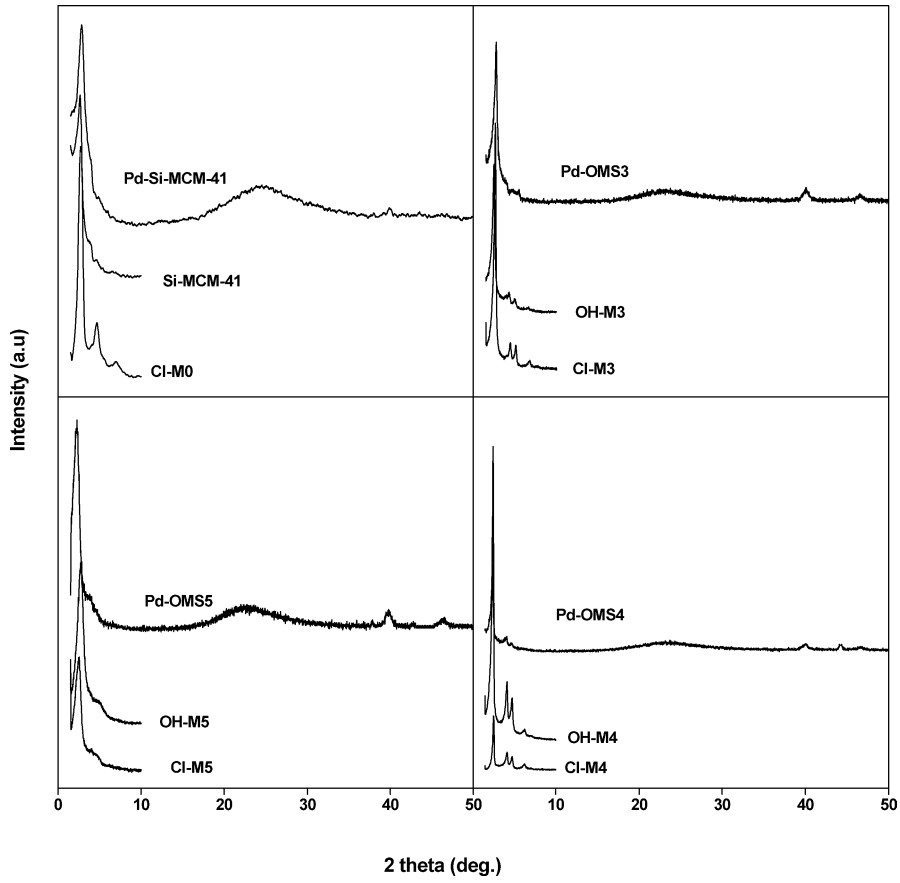

Fig. 2. X-ray diffraction patterns of Cl-M, OH-M, Si-MCM-41, Pd-OMS, and Pd–Si-MCM-41.

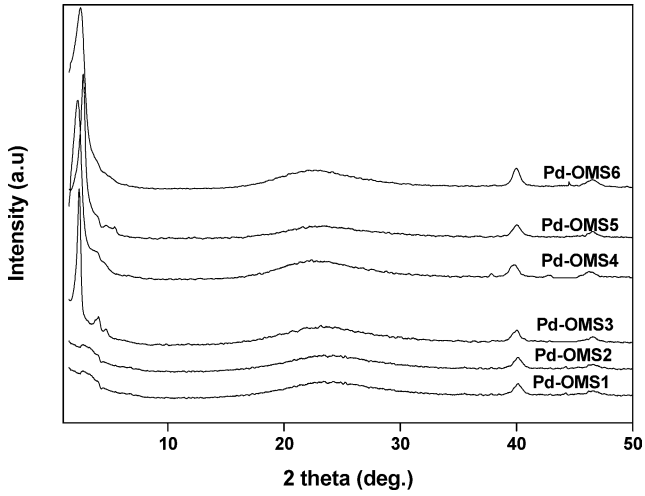

Fig. 3. X-ray diffraction patterns of Pd-OMS catalysts.

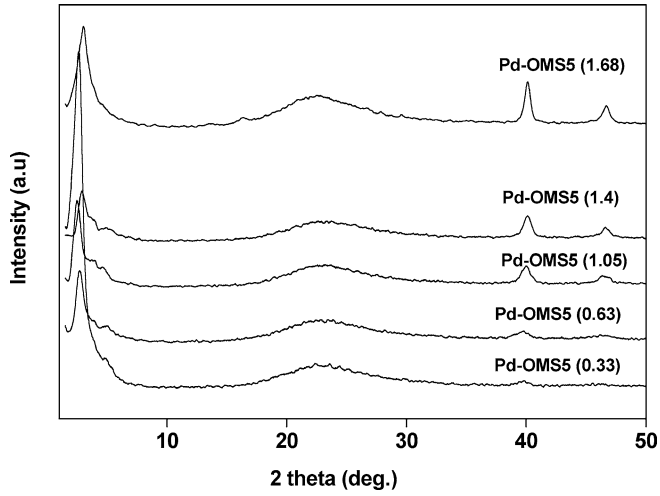

Fig. 4. X-ray diffractio patterns of Pd-OMS5 catalysts.

coordination of ligands proportionally increases with the concentration of ligands (3-ClPTS) in the material, which is evidence, that loading of palladium depends on the concentration of the ligand (Table 3). Total Pd content in the synthesized materials was achieved in the range of 0.3 to 1.7 wt%, which depended on both the loading of 3-ClPTS groups and the Pd concentration used in the reaction solution (Table 3). When similar concentrations of ligands are exposed to different concentrations of Pd, the uptake of Pd increases as the concentration of Pd increases in the solution up to a certain level and then it levels off. The maximum uptake of Pd reaches to 70% for catalyst Pd-OMS5 (1.05) and then it decreases to 40% when higher concentrations of Pd are used in the solution. Palladation with organo-functionalized silica also shows lower Pd uptake (0.25 wt% Pd) when compared to Pd-OMS5. The lower Pd uptake can be accounted for by

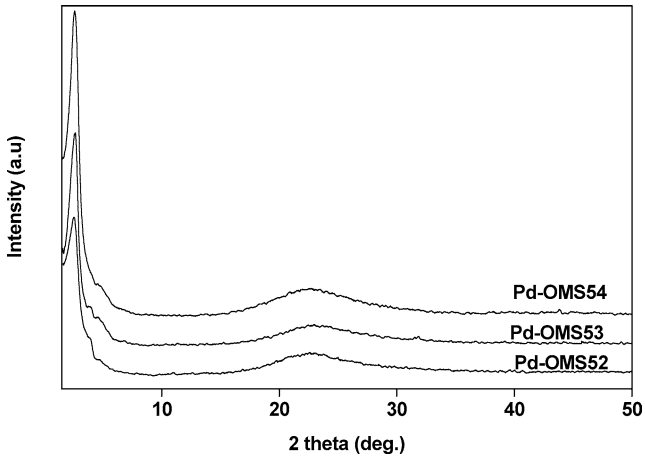

Fig. 5. X-ray diffraction patterns of Pd-OMS52, Pd-OMS53, and Pd-OMS54.

the slow palladation process over OH–SiO_2, as there is no spatial confinement as in the case of OH-M5.

The spatial confinement induced by the pore walls of OH–M drives the palladation more faster than in OH–SiO_2. The Pd content was lower in the materials, which were synthesized either at room temperature or without addition of base or with acetone as a solvent as compared to the material synthesized at 335 K and with the addition of base in methanol even though the reaction conditions are the same. Pd-OMS51, which was synthesized under room temperature, showed 0.32 wt% Pd whereas Pd-OMS5 (1.05) synthesized at 333 K showed 1.05 wt% Pd (Table 4). Similarly Pd-OMS52, which was synthesized without addition of base, showed a Pd content only 0.35 wt%. Pd-OMS54, which was synthesized with palladium acetate and $CHCl_3$ as a solvent at 335 K without addition of base, showed a Pd content 0.38 wt% but when the same one was synthesized at 333 K with addition of sodium acetate (Pd-OMS55) it showed 0.71 wt% Pd. Pd-OMS53, prepared with acetone as a solvent, shows a very low Pd uptake compared to the same one prepared with methanol solvent. The nonpolar solvent (acetone, 0.26 wt% Pd) favors palladation to lesser extent than the polar solvent (methanol, 1.05 wt% Pd).

From thermal studies, it was confirmed that additional complex formed exclusively when acetone was used as a solvent (exothermic peak around 673 K, Fig. 10c). These data clearly indicate that a palladium complex has been formed under mild reaction conditions irrespective of the solvent and base but at the same time the base and reaction temperature enhance not only the formation of palladacycle but also the reduction of palladium salt into Pd^0. So under the optimum reaction conditions, the formation of palladacycle is enhanced. For comparison unfunctionalized Si-MCM-41 was treated with palladation reagents and a much lower Pd uptake (0.14 wt% Pd) was found. This result clearly shows that propyl alcohol plays an important role in stabilizing Pd as Pd(II) in the palladacycle complex. C, H, and N analyses of the samples show that there is a linear increase in carbon content as we go from Cl-M1 to Cl-M6 catalysts (Table 3).

4.4. Adsorption studies

The surface areas of functionalized MCM-41 materials were in the range of 500–900 m^2/g, which are comparable to the previously reported organo-functionalized MCM-41 with organosilane functional groups [30]. Surface areas of OH-M1 and OH-M2 were 547 and 578 m^2/g, respectively. The lower surface area for OH-M1 and OH-M2 than for Cl-M1 (760 m^2/g) and Cl-M2 (735 m^2/g), respectively, is attributed to their decreasing long-range order, which is also evident from the XRD pattern. OH-M3, OH-M4, OH-M5, and OH-M6 materials do not show much difference in surface area, confirming that as the concentration of functionalized silicon atom increases the passive character of the silica walls toward acidic or basic solvent mixture also increases. The respective palladated catalysts show either similar or slightly higher surface areas. The surface area and average pore diameter as well as pore volume were found to increase when the material is palladated. The increase in surface area is attributed to the metal content and cyclization of groups inside the pores of MCM-41. The palladium, which enters into the pore, causes the pores to widen to accommodate it and therefore there is an increase in pore diameter as well as total pore volume (Fig. 6). The BJH (Braunauer–Joyner–Halenda) pore-size distribution of Pd-OMS5 illustrates a narrow peak centered at 28.8 Å for the pore diameter, and the pore volume measured was 0.63 cc/g. In case of pore-size distribution of OH-M5, the average pore diameter was in the range of 28.4 Å and the pore volume measured was 0.43 cc/g. The increase in pore volume might be due to enlargement of pore dimension due to the organo-functionalized groups. The nonbonding interactions between the organo-functionalized groups produce some kind of strain inside the pores, which triggers the pore walls to stretch outward and, hence, increase the pore volume as well pore diameter.

4.5. Fourier transform infrared spectra (FTIR)

Fig. 7 shows the FTIR spectroscopy of the as-synthesized Cl-M5, OH-M5, and Pd-OMS-5 materials. The OH-M5-containing propylalcohol group has a strong band in the region between 1300 and 800 cm^{-1}, assigned to the C–O stretching band and intense O–H stretching adsorption in the region of 3600–2500 cm^{-1}. In case of as-synthesized Cl–M5 sample, very strong stretching bands in the region 2950–2850 cm^{-1} and deformation bands in the region 1400–1420 cm^{-1} were observed. In the OH-M5 sample, the methylene stretching bands of the propyl chain, in the region 2950–2850 cm^{-1}, and their deformation bands, at 1414, 1440, 1475 cm^{-1}, are comparatively weaker (Fig. 7). These bands can be assigned to the symmetric bending ("scissoring") mode of the three distinct methylene groups of the

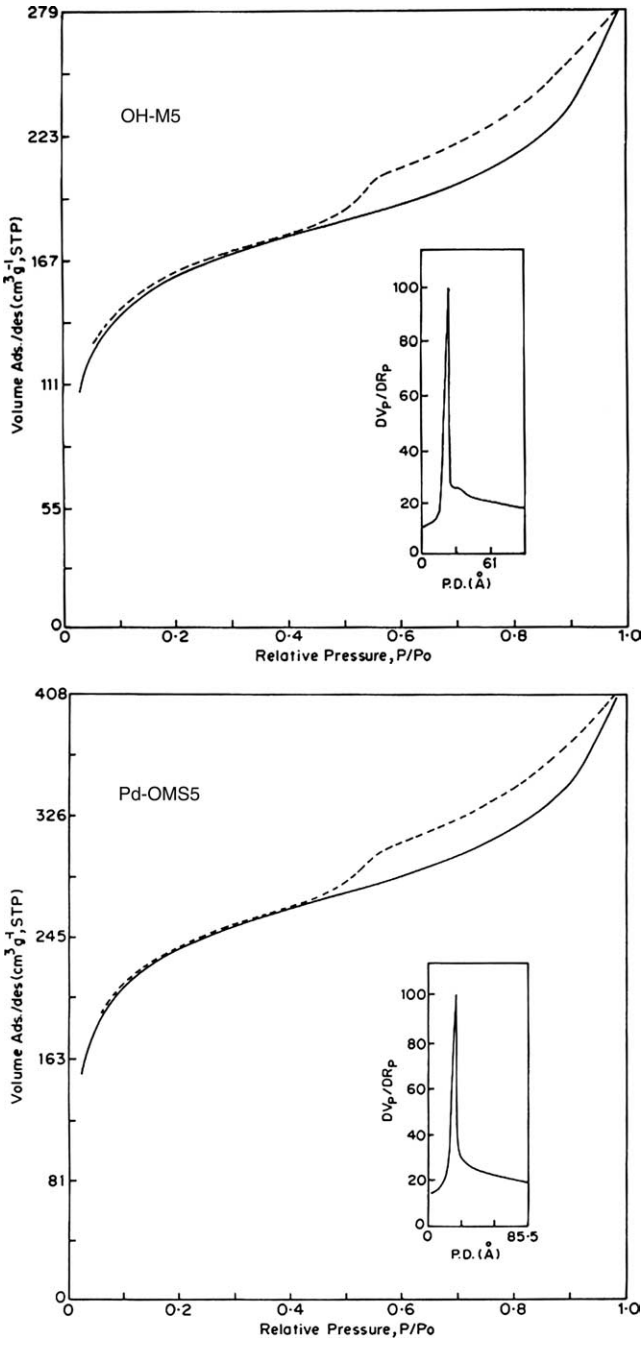

Fig. 6. Nitrogen adsorption–desorption isotherms and pore-size distribution (inset) of OH-M5 and Pd-OMS5.

propyl chain. The first one at 1416 cm^{-1} assigned to a methylene directly bonded to silicon [38] is also present in the palladated samples but the intensity is comparatively weak. After the palladation it was found that the intensity of the O–H stretching vibration also decreased. The C–H stretching bands also shifted from 2887 and 2941 cm^{-1} to 2894 and 2951 cm^{-1}, respectively, and one more extra band at 2851 cm^{-1} was also seen in Pd-OMS5. The shift toward the higher energy side indicates the change of bonding behavior of the C–H bond. These data provide supplemental

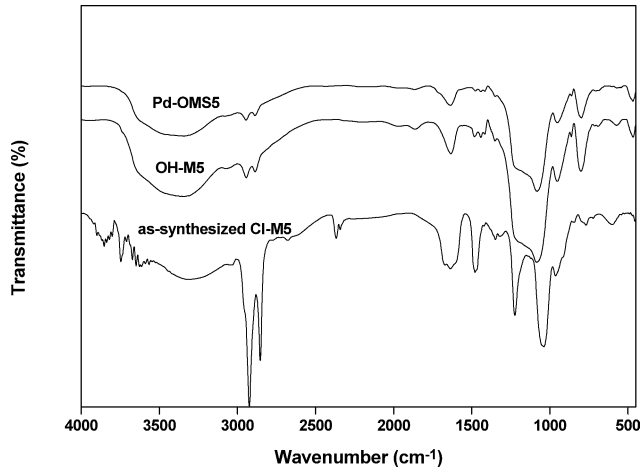

Fig. 7. FTIR spectra of as-synthesized Cl-M5, OH-M5, and Pd-OMS5.

evidence of the cyclometallation of the propyl alcohol group, which is anchored on the walls of MCM-41 in the presence of palladation reagents.

4.6. TGA-DTA analysis

The thermal stability of the palladated catalysts could be measured by TGA-DTA analysis. The weight losses observed for Cl-M5, OH-M5, and Pd-OMS5 (1.68) correspond to the loss of propylchloride, free propylalcohol, and complexed propylalcohol and are 30, 20, and 18 wt%, respectively (Fig. 8). It is clearly seen from the weight loss profile that 30 wt% loss corresponds to propylchloride which is reduced to 20 wt% due to propyl alcohol as expected. An exothermic peak centered at 280 °C in Cl-M5 is shifted to 300 °C in OH-M-5. The palladated sample Pd-OMS5 exhibits two broad peaks centered at 450 and 500 °C. The two exothermic peaks can be interpreted in such a way that the palladium complex formation with the ligands propylalcohol occurs in two different way. The exothermic peak at 500 °C can be assigned to the formation of palladacycle while the exothermic peak at 450 °C to the formation of additional complex (PdX_2L_2; L = ligand; X = –Cl or –OAc) [2–4]. When a similar concentration of ligands was treated with different concentrations of Pd, it was observed that at lower Pd concentrations, palladacycle predominates whereas at higher concentrations of Pd, additional complex as well palladacycle formed (Fig. 9). It was also observed that the exothermic peak (around 400–450 °C) assigned for the additional complex predominates when OH-M was treated without the addition of base at 335 K (Fig. 10c). Addition of base during synthesis catalyses the formation of palladacycle even at room temperature (Fig 10b). Pd-OMS54, prepared using acetone as a solvent shows two exothermic peaks at 410 and 520 °C (Fig 10). The uptake of Pd is lower in case of Pd-OMS54 as measured by ICP-OES analysis, and formation of additional complex predominates over palladacycle. These results suggest that palladacycle formation requires optimum reaction conditions and base. The polar solvent,

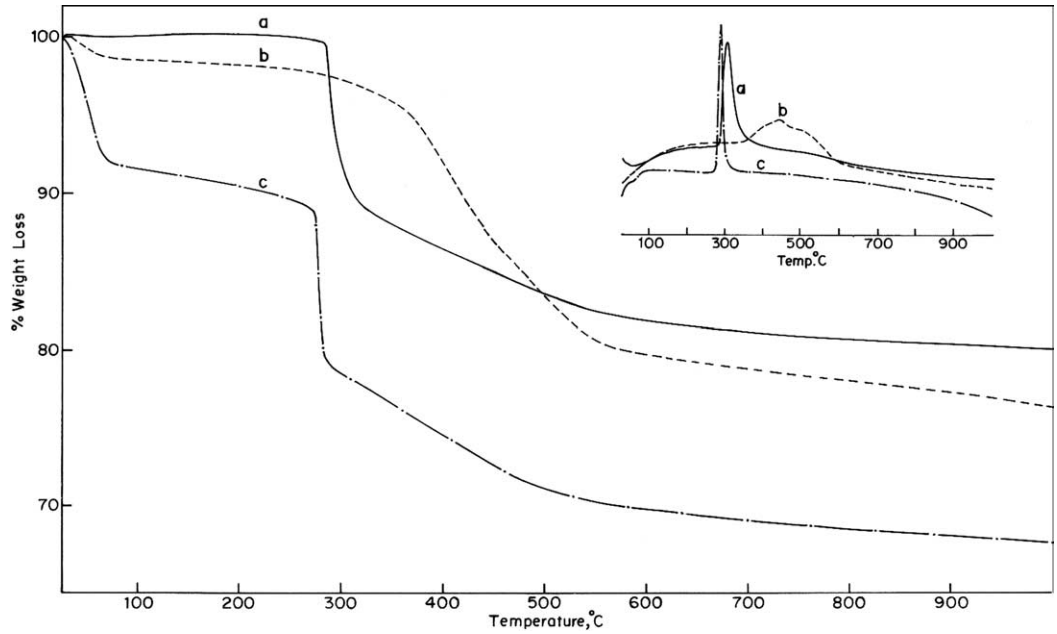

Fig. 8. TGA–DTA curves of (a) Cl-M5, (b) OH-M5, and (c) Pd-OMS5.

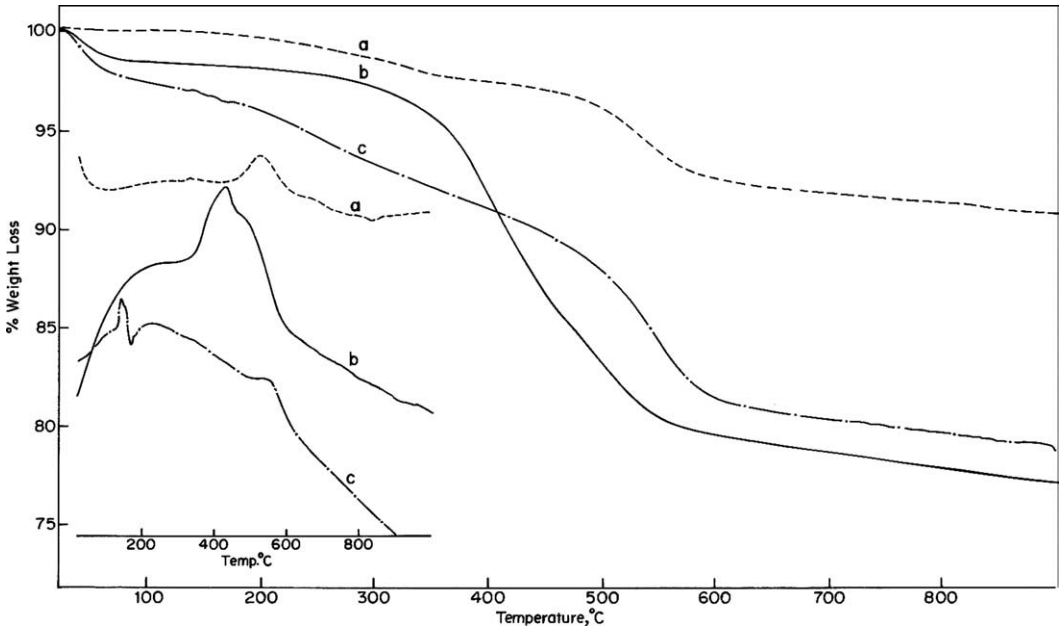

Fig. 9. TGA–DTA curves of (a) Pd-OMS5 (0.33), (b) Pd-OMS (1.68), and (c) Pd-OMS5 (1.05).

methanol, favors the formation of palladacycle at room temperature.

4.7. Electron microscopy

Scanning electron micrographs show the particle morphology of the samples. SEM photographs of OH-M5 and Pd-OMS5 shown in Fig. 11 are typical for mesoporous materials. Uniform particles sizes (1–2 μm) were present in OH-M5. Pd-OMS5 samples show particles sizes in the range of 1–3 μm. The same material when palladated under a different solvent system shows different morphologies. Pd-OMS53 that is prepared with acetone medium shows uniform spherical and cylindrical rod crystals.

4.8. Solid-state NMR studies

Fig. 12 shows the ^{29}Si NMR spectra of Pd-OMS5. The peak at 67.0 ppm is due to the cross-linked silicon atom. The concentration of cross-linked silicon atom is higher and hence the concentration of the Q_3 species along with the Q_4 species is accountable. In order to confirm the cyclic

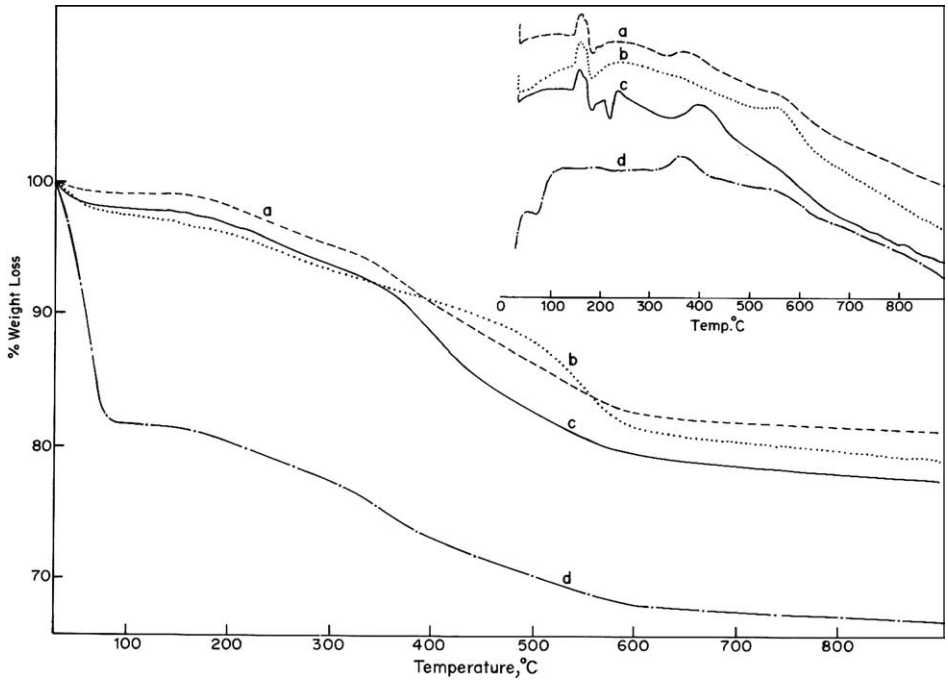

Fig. 10. TGA–DTA curves of (a) Pd-OMS5, (b) Pd-OMS51, (c) Pd-OMS52, and (d) Pd-OMS53.

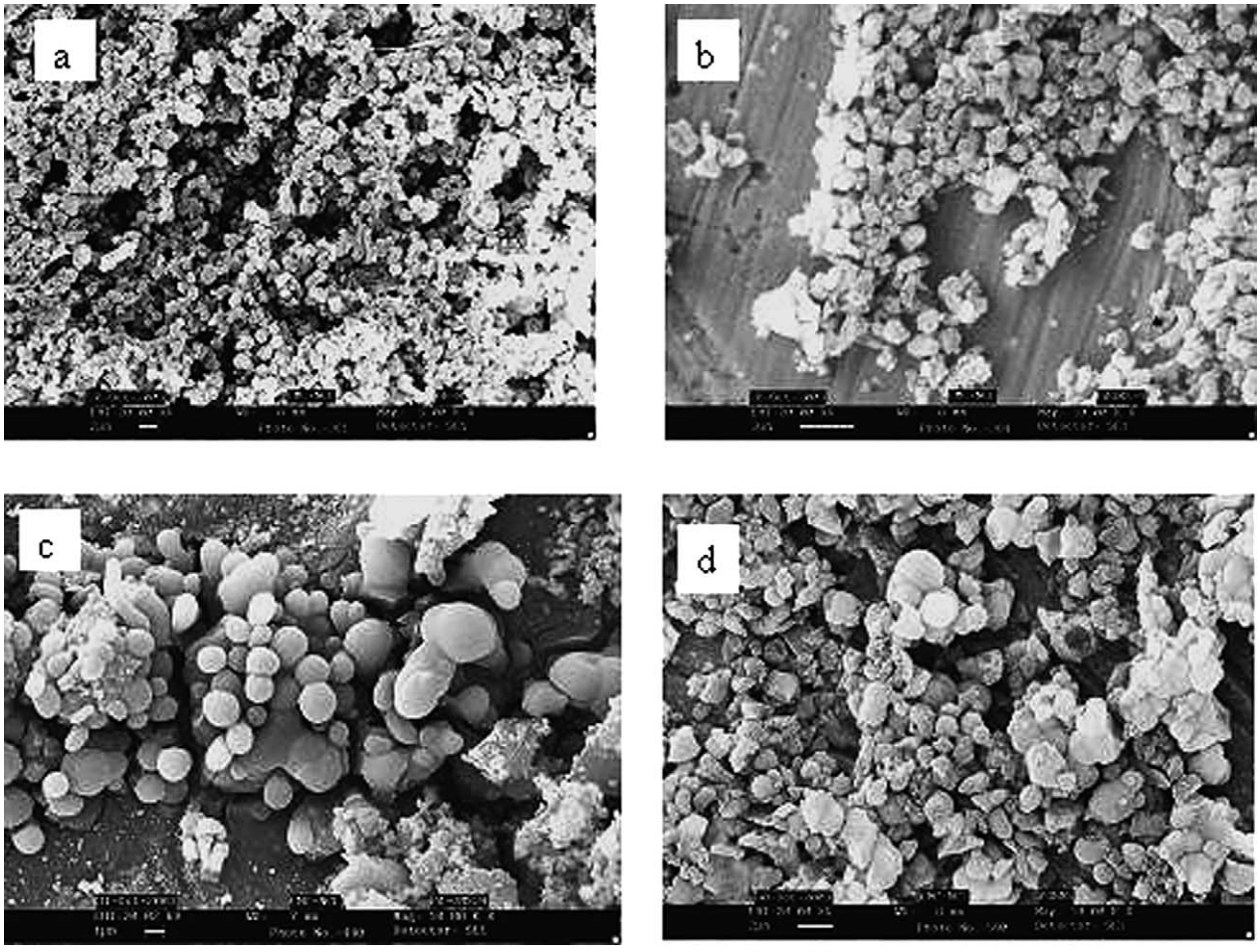

Fig. 11. SEM photographs of (a) OH-M5, (b) Pd-OMS5, (c) Pd-OMS53, and (d) Am-PdMS.

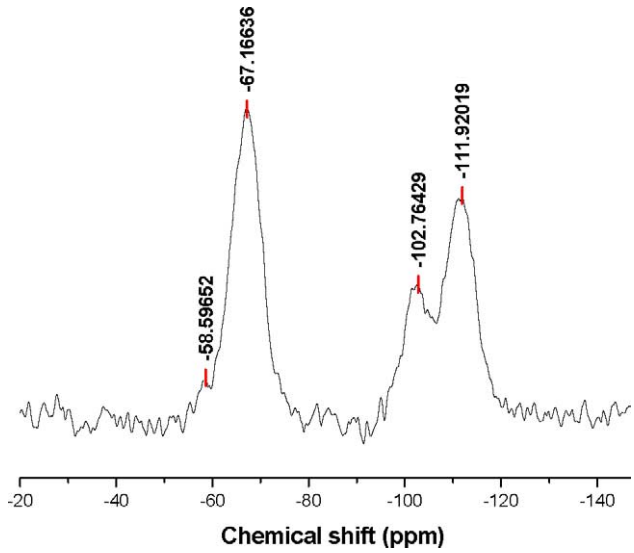

Fig. 12. ^{29}Si NMR spectra of Pd-OMS5 catalyst.

palladation with aliphatic carbon and oxygen of OH group, 125.76 MHz solid-state ^{13}C CP/MAS spectra of OH-MCM-41 and Pd-OMS have been recorded on a Bruker DRX-500 NMR spectrometer spun at 10 and 8 kHz, respectively, and are shown in Fig. 13. Three main peaks of OH-M5 observed at (δ) 8.67, 25.28, and 63.63 ppm have been shifted to 8.33, 25.368, and 63.65 ppm, respectively, in Pd-OMS5. The shift of methylene carbon next to the silyl silicon toward high field is sufficiently higher, 0.34 ppm, compared to that of the middle carbon and carbon atom neighbor to the OH group in Pd-OMS5. The shift of signal corresponding to methylene carbon next to silyl silicon to high field confirms that the carbon exhibited a different environment after palladation while the other two carbons do not show much difference. The shift toward high field confirms the complexation of the ligand with a Pd center.

Liquid-state ^{13}C NMR spectra of 3-aminopopyltriethoxysilane in $CDCl_3$ and APTES + $Pd(OAc)_2$ have been recorded on a Bruker 300 MHz instrument to evidence the formation of a Pd complex (Fig. 14). APTES shows three well-distinct peaks (C_1, C_2, and C_3 at 7.16, 26.72, and 44.54 ppm, respectively) corresponding to the three carbons of the propyl group. When the APTES is added with palladium acetate and heated at 333 K for 24 h, it shows broader and almost invisible peaks corresponding to carbons C_1 and C_3, strongly confirming the formation of complex. A peak at 26.72 ppm corresponding to C_2 carbon of the propyl group in APTES is found shifted toward higher field (24.7 ppm) after palladation. Though the shift is not much as in case of completely complexed solid, this shift suggests that there is an equilibrium existing between partly complexed and uncomplexed ligand and hence the shift is not much. The peaks at 17.78 and 57.85 ppm correspond to C_1 ($-CH_3$) and C_2 ($-CH_2$) carbon of ethoxy groups in APTES, respectively. This analysis confirms the formation of a

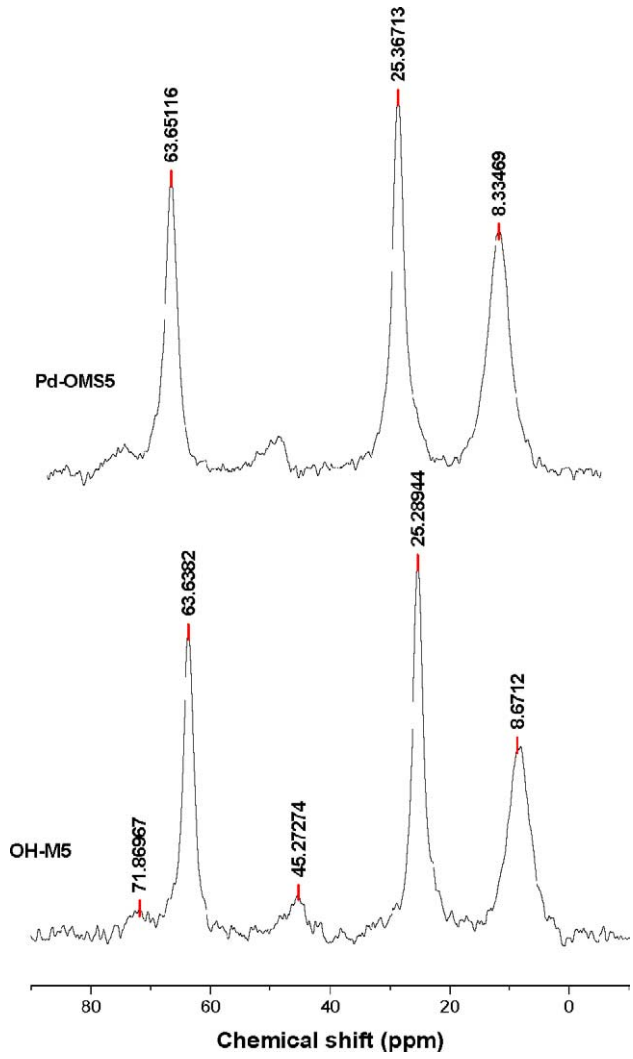

Fig. 13. ^{13}C CP MAS NMR spectrum of OH-M5 and Pd-OMS5.

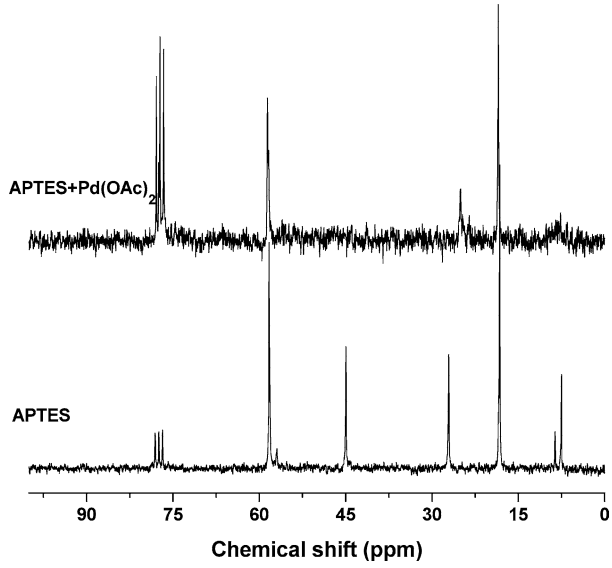

Fig. 14. Liquid-state ^{13}C NMR spectra of APTES and $Pd(OAc)_2$ + APTES in $CDCl_3$.

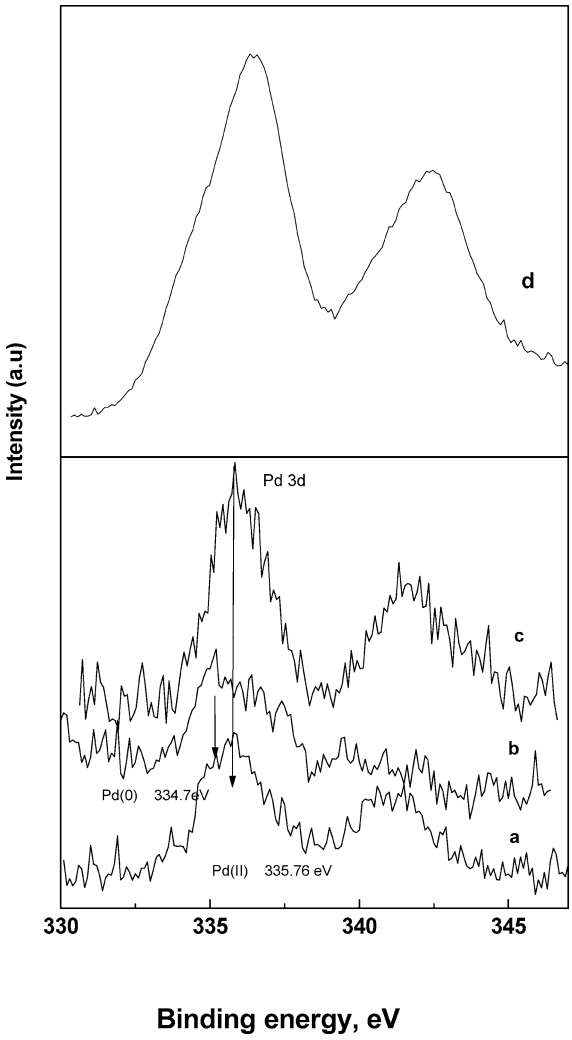

Fig. 15. XPS spectra of (a) Pd-OMS5 (1.4), (b) Pd-OMS54, (c) Pd-OMS51, and (d) Am-PdMS.

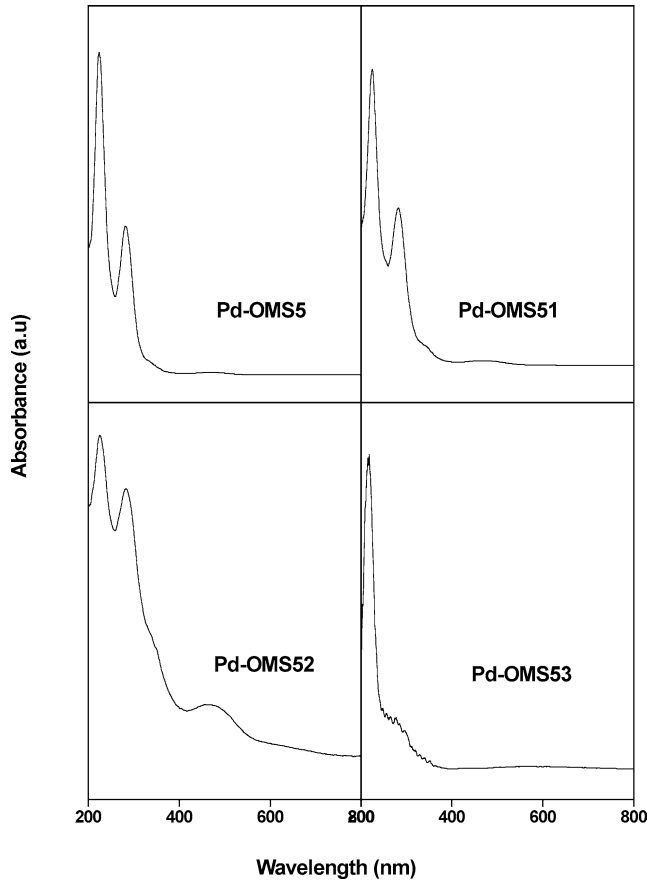

Fig. 16. UV–vis spectrum of Pd-OMS5, Pd-OMS 51, Pd-OMS52, and Pd-OMS53.

palladacycle complex with 3-aminopropylsilyl ligands anchored onto the walls of MCM-41.

4.9. XPS studies

Pd (3d) XPS spectra of Pd-OMS5 (1.4), Pd-OMS51, Pd-OMS54, and Am-PdMS support the formation of palladacycle (Fig. 15). The binding energy of adventitious C 1s core level, which is 284.6 eV [39], was used to correct for the energy shift due to the surface charge. The accuracy of the measured BE was ±0.2 eV. The peak maximum of the Pd(II) $3d_{5/2}$ line for all the samples except Am-PdMS is centered around 336 eV. Pd-OMS5 (1.4) shows a weak Pd(0) $3d_{5/2}$ line at a binding energy of 334.7 eV, which is found to be absent for other samples. Palladium present in palladacycle is in the Pd(II) form and the binding energy is slightly lower compared to Pd(II) in PdO (335.6 eV). Pd-OMS54 prepared with $Pd(OAc)_2$ in chloroform at 335 K shows no shoulder corresponding to Pd (0) on its surface whereas Pd-OMS5 (1.4) prepared with Li_2PdCl_4 as Pd source at 333 K with methanol as a solvent and sodium acetate as base shows a weaker band at 334.7 eV which is a characteristic binding energy of Pd(0). Pd-OMS51 prepared at room temperature shows a clear peak corresponding to Pd(II) at 336.4 eV (Fig. 15c). Similarly Am-PdMS shows a clear and sharp peak at 337.6 eV confirming the formation of highly stable palladacycle (Fig. 15d).

4.10. UV–vis spectra

The diffuse reflectance spectra (200–800 nm) of Pd-OMS catalysts display nearly identical features with three absorption bands in the UV region in the range 260 and 450 nm with reference to $BaSO_4$ standard (Fig. 16). Pd-OMS5 shows a characteristic absorption band at 284 nm corresponding to a metal–ligand charge transfer d–p transition. The shift toward higher energy values result from the metallation. When the palladation was carried out at room temperature over OH-M5, an intense absorption band around 281 nm indicates the formation of palladacycle exclusively. A weak shoulder at 346 nm followed by the intense band may be due to little formation of additional complex. The absorption band around 346 nm was more visible along with one more broad band at 475 nm when the OH-M5 was palladated without the addition of base at 335 K. Palladation with

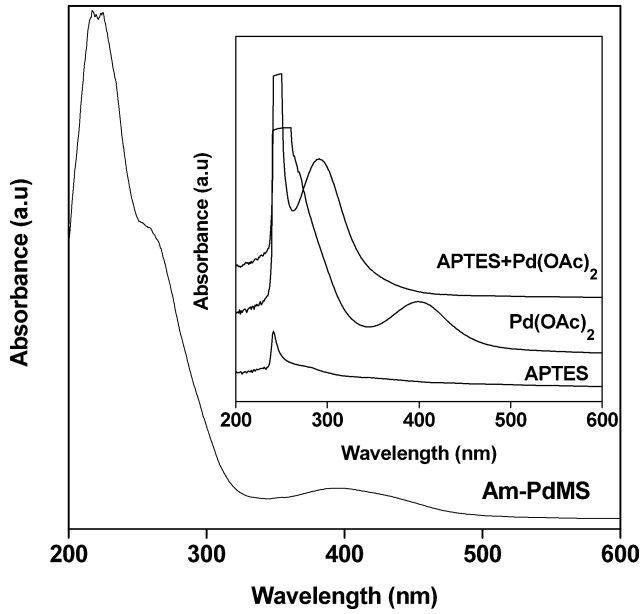

Fig. 17. UV–vis spectrum of APTES, $Pd(OAc)_2$, APTES + $Pd(OAc)_2$ in $CHCl_3$, and Am-PdMS.

acetone as a solvent shows a weak but exclusive absorption band corresponding to the rigid palladacycle.

To confirm the above fact, UV–vis spectra of APTES in $CHCl_3$ solvent were recorded before and after the addition of palladium acetate into APTES to evidence the complexation. In the DR-UV–vis spectrum, it is clearly seen that the absorbance band for the neat palladium acetate in $CHCl_3$ at 400 nm is shifted to 300 nm when subjected to complexation with APTES ligand (Fig. 17). The blue shift is clear evidence of the formation of Pd complex. In the DR-UV–vis spectrum of solid Am-PdMS, the most characteristic absorption bands at 261 and 400 nm indicate the formation of a rigid palladium complex and a nonrigid additional complex. The blue shift found in case of solid Am-PdMS catalyst (139 nm) is higher than that of Pd complex in $CHCl_3$ solution (100 nm) as there are higher degrees of freedom for liquid than solid. The absorption spectrum of neutral palladium(II) complexes is generally characterized by a ligand–metal charge transfer d–p transition. The observed spectral features are consistent with Pd(II) [d^8] diamagnetic species [40]. These results confirm the formation of a rigid palladacycle and a nonrigid additional complex when OH-M5 or Am-MCM-41 was treated with palladation reagents even under mild reaction conditions.

4.11. Heck alkenylation of bromobenzene

Heck alkenylation of BB with styrene has been performed to evaluate the catalysts prepared under different reaction conditions (Scheme 2). Palladacycle–SiO_2 shows lower activity for the conversion of BB. The uptake of Pd is consequently signified in the Heck alkenylation reaction (Fig. 18). Under similar reaction conditions the conversion and TON increase linearly from Pd-OMS1 to Pd-OMS5 and thereafter decrease, which implies exceeding the optimum loading of 3-ClPTS groups. As the reaction proceeds at the active Pd metal center, the TON (with respect to Pd) varies significantly when the Pd content is changed. The Pd uptake increases proportional to the amount of ligand (3-hydroxypropyltriethoxysilane) present in the mesoporous walls of MCM-41 and so the rate of reaction (TON) increases accordingly. As can be seen from Table 3, though the Pd content (wt%) is higher in Pd-OMS2 than in Pd-OMS4 the activity was lower which might be attributed to the formation of bulk Pd in Pd-OMS2, which is catalytically inactive for such reaction. The same fact also was observed in Pd-OMS3 where the Pd content was higher than those of Pd-OMS4 and Pd-OMS5 but found to be less active. From these experiment it was clearly seen that whenever there are fewer ligands available for the formation of palladacycle, the excess palladium present in the solution tends to deposit at the surface of silica near to the anchoring point of the functional group. To confirm this fact, palladation was performed with Si-MCM-41 (where there is no functional group) under similar reaction conditions and it was found that uptake of palladium in the form of bulk Pd was substantially low as seen in XRD which is inactive for this reaction. In order to study the effect of base and reaction temperature palladation was performed with and without the addition of base either at room temperature or at 333 K. Palladacycle prepared at room temperature shows a lower Pd content (wt%) but moderate activity. The catalytic activity of Pd-OMS54 prepared with palladium acetate with chloroform solvent was found to be lower when compared to the one prepared with base and at 333 K (Pd-OMS55). Table 4 shows the effect of Pd (wt%) loading over OH-M5 in the Heck alkenylation reaction. When OH-M5 was treated with different concentrations of Pd-containing solution, the uptake of Pd increased up to 70% and then started to decrease. Conversion of bromobenzene increases as the Pd content increases in the catalyst. A maximum of 1.68 wt% Pd content in the catalyst (Pd-OMS5 (1.68) was achieved but at the same time the catalyst shows less activity in the conversion of bromobenzene than Pd-OMS5 (1.4) containing 1.4 wt% Pd. This result confirms that the activity of Pd arises only from Pd present as Pd(II) in palladacycle and not from bulk Pd deposited on the surface.

4.12. Study of the heterogeneous nature of the Pd-OMS5

To analyze the heterogeneity of the catalyst, a reaction was performed with PdOMS5 catalyst. After attaining 20% conversion of bromobenzene, a 5-ml reaction mixture was filtered and the reaction was performed in a separate reaction setup. After filtering the sample, the reaction was continued further up to 24 h. A higher conversion of 36% of bromobenzene could be achieved with tributylamine as a base. The conversion of bromobenzne was lower when tributylamine was used as a base. Even though K_2CO_3 gave > 90% conversion, tributylamine was chosen to study the leaching of Pd at a slower conversion rate and also organic amine was

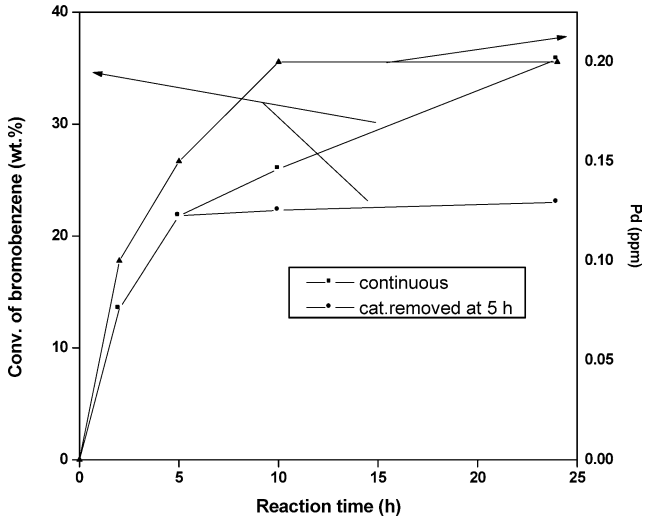

Fig. 18. Heck alkenylation of bromobenzene; reaction conditions: BB $= 1 \times 10^{-2}$ mol; styrene $= 1.5 \times 10^{-2}$ mol; tributylamine $= 1.2 \times 10^{-2}$ mol; NMP $= 25$ ml; temperature $= 423$ K; catalyst $= 0.1$ g.

equally mixed with the reactant mixture rather than K_2CO_3. The Pd content present in the solution was measured by ICP-OES analysis and it was found that a 0.2 ppm level of Pd was present in the solution. However, this Pd can be accounted for by bulk Pd present in the catalyst surface that may get leached out during the reaction and not the cyclized Pd. This fact can also be confirmed by the reaction performed with the reaction mixture, which was separated after a 5-h reaction time and shows no increase in conversion.

The maximum concentration of organo-functionalized groups inside the mesopores was achieved through in situ hydrolysis of TEOS and 3-ClPTS and successive cocondensation of respective monomer silica species. It was observed through optimization studies that the uptake and stabilization of Pd in palladacycle depend on both the concentration of ligands tethered on silica walls and the concentration of Pd in the reaction medium. As seen in ICP analysis the palladium content increases with the concentration of ligands anchored onto the walls of mesoporous materials up to certain extent and then it levels off. Loading of Pd as palladacycle depends mainly on the reaction conditions. The polar solvent, methanol, favors formation of palladacycle with sodium acetate as base under mild reaction conditions. Higher reaction temperatures enhance the deposition of bulk Pd along with the formation of palladacycle, which is observed in XRD and XPS. The nonpolar solvent, acetone, favors only additional complex under similar reaction conditions as evident from thermal analysis. The formation of rigid palladacycle and nonrigid additional complex is characterized by means of characteristic absorption bands in the UV–vis region. Solid-state and liquid-state ^{13}C NMR studies confirm the formation of a palladacycle complex. Pd-OMS5 (1.4) having 1.4 wt% Pd exhibited higher activity in the conversion of bromobenzene to *trans*-stilbene. Heterogeneity study reveals that leaching of Pd from the complex into the solution is much lower (0.2 ppm) and could be used as a heterogeneous coupling catalyst.

5. Conclusion

Heterogeneous carbometallated palladacycle has been successfully synthesized by treatment of palladation reagents with 3-hydroxypropyltriethoxysilane-incorporated MCM-41 (OH-M) under mild reaction conditions. The spatial confinement induced by the pore walls drives the palladation process. A number of characterization techniques supported the formation of a palladacycle complex inside the pores of mesoporous materials. Among the catalysts screened for Heck alkenylation of bromobenzene, Pd-OMS5 (1.4) having 1.4 wt% Pd exhibited higher activity in the conversion of bromobenzene to *trans*-stilbene. Heterogeneity study reveals that leaching of Pd from the complex into the solution is much lower (0.2 ppm) and could be used as a heterogeneous coupling catalyst.

Acknowledgments

C.V. thanks the Council for Scientific and Industrial Research (CSIR), New Delhi, for granting a senior research fellowship. The authors thank Drs. C.S. Gopinath, P.R. Rajamohanan, N.E. Jacob, and Mr. R. Marimuthu, S.P. Gaikwad, Jha, N. Vasudev Shetty, P.R. Selvakannan, and M. Chidambaram for their valuable contributions and cooperation in characterizing the catalysts and CSIR, New Delhi (Task force project, P23-CMM 0005B) for financial support.

References

[1] R.F. Heck, Palladium Reagents in Organic Syntheses, Academic Press, London, 1985;
J. Tsuji, Palladium Reagents and Catalysts, Wiley, Chichester, 1995;
I.P. Beletskaya, A.V. Cheprakov, Chem. Rev. 100 (2000) 3009.
[2] W.A. Hermann, C. Brossmer, K. Ofele, C.-P. Reisinger, T. Priermeir, M. Beller, H. Fischer, Angew. Chem. Int. Ed. Engl. 34 (1995) 1844.
[3] M. Beller, H. Fischer, W.A. Hermann, K. Ofele, C. Brossmer, Angew. Chem. Int. Ed. Engl. 34 (1995) 1848.
[4] W.A. Hermann, M. Elison, J. Fischer, C. Kocher, G.R.J. Artus, Angew. Chem. Int. Ed. Engl. 34 (1995) 1844.
[5] W. Cabri, I. Candiani, Acc. Chem. Res. 28 (1995) 2.
[6] B.L. Shaw, S.D. Perara, E.A. Staley, Chem. Commun. (1998) 1361.
[7] F. Miyazaki, K. Yamaguchi, M. Shibasaki, Tetrahedron Lett. 40 (1999) 7379.
[8] M.T. Reetz, E. Westermann, R. Lohmer, G. Lohmer, Tetrahedron Lett. 39 (1998) 8449.
[9] W.A. Hermann, V.P.W. Bohm, C.P. Reisinger, J. Organomet. Chem. 576 (1999) 23.
[10] A. Biffis, M. Zecca, M. Basato, J. Mol. Catal. A: Chem. 173 (2001) 249.
[11] J. Zhou, R. Zhou, L. Mo, S. Zhao, X. Zheng, J. Mol. Catal. A: Chem. 178 (2002) 289.
[12] B.M. Bhanage, M. Arai, Catal. Rev. 43 (2001) 315.
[13] A. Biffis, M. Zecca, M. Basato, Eur. J. Inorg. Chem. 5 (2001) 1131.

[14] C.M. Anderson, K. Karabelas, A. Hallberg, J. Org. Chem. 50 (1985) 3891.
[15] P.W. Wang, M.A. Fox, J. Org. Chem. 59 (1994) 5358.
[16] R.L. Augustine, S.T. O'Leary, J. Mol. Catal. A: Chem. 95 (1995) 277.
[17] B.M. Choudary, S. Madhi, N.S. Choudari, M.L. Kantam, B. Sreedhar, J. Am. Chem. Soc. 124 (2002) 14127;
S.S. Prockl, W. Kleist, M.A. Gruber, K. Kohler, Angew. Chem. Int. Ed. Engl. 43 (2004) 1881.
[18] T.H. Bennur, A. Ramani, R. Bal, B.M. Chanda, S. Sivasanker, Catal. Commun. 3 (2002) 493.
[19] M. Dams, L. Drijkoningen, B. Pauwels, G. Van Tendeloo, D.E. De Vos, P.A. Jacobs, J. Catal. 209 (2002) 225.
[20] L. Djakovitch, K. Koehler, J. Am. Chem. Soc. 123 (2001) 5990.
[21] C.T. Kresge, M.E. Leonowicz, W.J. Roth, J.C. Vartuli, J.S. Beck, Nature 359 (1992) 710.
[22] C.P. Mehnert, D.W. Weaver, J.Y. Ying, J. Am. Chem. Soc. 120 (1998) 12289.
[23] H. Kosslick, I. Mönnich, E. Paetzold, H. Fuhrmann, R. Fricke, D. Müller, G. Oehme, Micropor. Mesopor. Mater. 44–45 (2001) 537.
[24] R.B. Bedford, C.S.J. Cazin, M.B. Hursthouse, M.E. Light, K.J. Pike, S. Wimperis, J. Organomet. Chem. 633 (2001) 173.
[25] A.J. Sandee, D. Dimitrijevic, R.J. van Haaren, J.N.H. Reek, P.C.J. Kamer, P.W.N.M. van Leeuwen, J. Mol. Catal. A: Chem. 182–183 (2002) 309.
[26] C. Baleizao, A. Corma, H. Garcia, A. Leyva, Chem. Commun. (2003) 606.
[27] H.H. Wagner, H. Hausmann, W.F. Hölderich, J. Catal. 203 (2001) 150.
[28] V.V. Dunia, L.G. Kuz'mina, M.Y. Kazakova, O.N. Gorunova, Y.K. Grishin, E.I. Kazakova, Eur. J. Inorg. Chem. (1999) 1029.
[29] C. Venkatesan, A.P. Singh, Catal. Lett. 88 (2003) 193.
[30] C. Venkatesan, A.P. Singh, unpublished results.
[31] R. Anwander, I. Nagl, M. Widenmeyer, G. Engelhardt, O. Groeger, C. Palm, T. Roser, J. Phys. Chem. B 104 (2000) 3532.
[32] J.H. Clark, D.J. Macquarrie, Chem. Commun. (1998) 853.
[33] X.S. Zhao, G.Q. Lu, J. Phys. Chem. B 102 (1998) 1556.
[34] J. Vicente, I. Saura-Liamas, M.G. Palin, P.G. Jones, J. Chem. Soc., Dalton Trans. (1995) 2535.
[35] H.M. Hultman, M. de Lang, M. Nowotny, I.W.C.E. Arends, U. Hanefeld, R.A. Sheldon, T. Maschmeyer, J. Catal. 217 (2003) 264.
[36] V.V. Dunia, O.A. Zalevskaya, V.M. Potapov, Ruus. Chem. Rev. (Engl. Transl.) 57 (1988) 434.
[37] A.L. Seligson, W.C. Trogler, J. Am. Chem. Soc. 113 (1991) 2520.
[38] N.P.G. Roeges, A Guide to the Complete Interpretation of Infrared Spectra of Organic Structures, Wiley, Chichester, 1994.
[39] C. Battistoni, V. Cantelli, M. Debenedetti, S. Kaciulis, G. Mattogno, A. Napoli, Appl. Surf. Sci. 144–145 (1999) 390.
[40] D.S. Martin, R.M. Rush, G.A. Robin, Inorg. Chem. 19 (1980) 1705.